

Versatile formation of Ru(II) hydrazone complexes: Structure, theoretical studies and catalytic activity in α -alkylation



Kaliyappan Murugan, Subbarayan Vijayapritha, Venkatachalam Kavitha, Periasamy Viswanathamurthi *

Department of Chemistry, Periyar University, Salem 636 011, India

ARTICLE INFO

Article history:

Received 19 March 2020

Accepted 1 August 2020

Available online 13 August 2020

Keywords:

Ru(II) hydrazone complexes

Crystal structure

Hirshfeld surface analysis

DFT calculations

α -Alkylation

ABSTRACT

New 1-(anthracen-10-yl)methylene)-2-(benzo[d]thiazol-2-yl)hydrazine (**BHA**) and 1-(anthracen-10-yl)methylene)-2-(quinolin-2-yl)hydrazine (**QHA**) ligands were reacted with $[\text{RuCl}(\text{CO})(\text{E})_3]$ ($\text{E} = \text{PPh}_3$ or AsPh_3) or $[\text{RuCl}_2(\text{AsPh}_3)_3]$ in a 1:1 mol ratio in chloroform-ethanol medium to synthesize new ruthenium complexes. All the new ruthenium complexes were analyzed by elemental analysis, IR, NMR (^1H , ^{13}C and ^{31}P) spectroscopy, ESI-Mass spectrometry and single crystal XRD techniques. The single crystal XRD study reveals the octahedral geometry around the ruthenium ion. The study also shows that the ligands coordinate with the Ru metal as monoanionic bidentate N^N donors in complexes **1**, **3** and **4** and as a neutral bidentate N^N donor in complex **2** by forming five or four member chelate rings. The intramolecular interactions in the crystal lattices were studied by Hirshfeld surface analysis. The results indicate that π -stacking contacts play an important role in the crystal lattices. DFT calculations were carried out to explain the solid structures of complexes **1–3**. Moreover, the synthesized complexes were screened as catalysts for the α -alkylation of ketones with alcohols. The effect of various parameters, such as base, solvent, temperature, time, substituents and also catalyst loading, on the catalytic activity were analyzed. The results depict that the complex **3** was found to be an efficient catalyst for the synthesis of α -alkylation products.

© 2020 Elsevier Ltd. All rights reserved.

1. Introduction

The construction of carbon-carbon bonds by the α -alkylation of ketones with alcohols, catalyzed by transition metal complexes, has occupied a special place in synthetic organic chemistry [1]. Conventionally, α -alkylation reactions were carried out by the reaction of enolates or enamines obtained from ketones with carbon electrophiles, such as alkyl halides [2,3]. However, a pre-functionalization step and a stoichiometric excess amount of base, generating an equivalent amount of salt as waste, were required for above nucleophilic substitution [4]. These drawbacks prompted us to develop an alternative protocol to achieve the same objective. Borrowing-hydrogen methodology (BH) is one of the methods has been given attention in recent years for the alkylation of ketones catalyzed by transition-metal catalysts [5]. Such reactions release water as the only by-product and hence are environmentally benign, in addition to being highly atom economical [6]. In BH methodology, initially alcohols are converted into the corresponding carbonyl compounds by oxidation, then unsaturated compounds are formed by alkylation of the ketones. Finally borrowed hydrogen atoms from alcohols are used for reduction of the C—C bonds.

In connection with the BH methodology, hitherto Ru and Ir complexes have been used as the most effective catalysts for the alkylation of ketones with alcohols [7]. Among the early reports, the $\text{RuCl}_2(\text{PPh}_3)_2$ catalyst was reported for the α -alkylation of ketones with primary alcohols by Cho et al [8]. In the reported catalytic reaction, 1-dodecene was added as the hydrogen acceptor to arrest the formation of α -alkylated alcohols via further hydrogenation of alkylated ketones. Yus et al proved $\text{RuCl}_2(\text{DMSO})_4$ was an efficient catalyst for the α -alkylation of ketones with benzylic alcohols in the presence of a stoichiometric amount of base [9]. An efficient catalytic system, $[\text{Ir}(\text{cod})\text{Cl}]_2/\text{PPh}_3/\text{KOH}$, under solvent-free conditions was developed by Ishii et al to accomplish α -alkylation [10]. More recently, Ryu's group developed an efficient $\text{RuHCl}(\text{CO})(\text{PPh}_3)_3/\text{Cs}_2\text{CO}_3$ system for α -alkylation of acetophenones [11,12]. The alkylation of ketones with primary alcohols catalyzed by ruthenium(II)/P,N ligand complexes was reported by Jiang et al. [13]. Several P, N ligands were screened in this reaction to study the steric hindrance and electronic effects. Smith et al [14] described the ruthenium catalyzed α -alkylation of ketones using pyridyl methanol, in which there is no need for addition of hydrogen receptors or the use of a stoichiometric amount of base. Apart from the homogeneous catalysts, several recyclable heterogeneous catalyst systems have been developed and investigated extensively in recent years [15].

* Corresponding author.

E-mail address: viswanathamurthi@gmail.com (P. Viswanathamurthi).

Generally, in development of transition metal catalysts for a specific process, besides choosing the right metal ion, the design of the ligand is also very important. Since the nature of the ligand has a profound effect on the coordination chemistry of a metal complex, the design and “tailoring” of the ligand properties can lead to complexes with efficient homogeneous catalytic activities. In this connection, Schiff-base ligands have gained significant attention due to their rich coordination chemistry. In particular, Schiff base ligands possess the main advantages like being easily accessible under gentle conditions, readily facilitating adjustment of their structures and chemo-physical properties through the incorporation of some additional functional groups. On coordination of Schiff bases with metal ions, the resulting complexes exhibit numerous applications in catalysts [16], pharmaceuticals [17] and magnetic materials [18].

Given such considerations and inspired by the high activity of Ru(II) complexes in α -alkylation reactions, in addition to our systematic investigation to find effective homogeneous catalysts [19,20], herein we report the design and synthesis of hydrazone Schiff base ligands and their ruthenium(II) complexes. The coordination modes of the ligands with ruthenium metal were investigated using FT-IR, NMR (^1H , ^{13}C and ^{31}P) spectroscopy and mass spectrometry. The solid-state structures of the complexes were established by single-crystal X-ray diffraction. The catalytic properties of the new complexes were screened for the α -alkylation of ketones with alcohols.

2. Experimental

2.1. Materials and instrumentation

All the reagents used were of Analar grade. $\text{RuCl}_3 \cdot x\text{H}_2\text{O}$, anthracene 9-carbaldehyde, mercaptobenzothiazole and 2-chloro quinoline were purchased from Sigma Aldrich. Solvents were dried by the reported procedures [21]. Elemental analyses were performed using a Vario EL III elemental analyzer. The IR spectra of the ligands and the complexes were recorded with a Bruker-alpha instrument in the 4000–600 cm^{-1} range. NMR (^1H , ^{13}C and ^{31}P) spectra were measured in CDCl_3 with a Varian AMX 400 instrument using tetramethyl silane (^1H , ^{13}C) or *o*-phosphoric acid (^{31}P) as an internal standard. Electro spray ionization mass spectra were measured using a liquid chromatography mass spectrometry quadrupole time-of-flight Micro Analyzer (Shimadzu) at the Indian Institute of Technology, Chennai. Column chromatography purifications were performed for the complexes using silica mesh 100–200 mesh. Melting points were recorded on a Lab India melting point apparatus. The starting precursors $[\text{RuHCl}(\text{CO})(\text{PPh}_3)_3]$, $[\text{RuHCl}(\text{CO})(\text{AsPh}_3)_3]$ and $[\text{RuCl}_2(\text{AsPh}_3)_3]$ were prepared according to the published literatures [22–24].

2.2. General procedure for synthesis of the hydrazone ligands

The ligands were synthesized by the following general procedure. 9-Anthracenecarboxaldehyde (1 mmol) was added to the hydrazines (1 mmol) in ethanol (20 mL) and the reaction mixture was subsequently refluxed for 6 h. After completion of the reaction, a solid compound formed, which was filtered, washed with ether and dried in air.

2.2.1. 2-(2-(Anthracen-9-ylmethylene)hydrazinyl)benzo[d]thiazole (BHA)

This was prepared from 9-anthracenecarboxaldehyde (0.206, 1 mmol) and 2-hydrazinyl benzo[d]thiazole (0.165 mg, 1 mmol). Yield: 77%. Color: Yellow. M.p.: 260 °C. Anal. Calcd. for $\text{C}_{22}\text{H}_{15}\text{N}_3\text{S}$: C, 74.76; H, 4.28; N, 11.89; S, 9.07. Found: C, 74.82;

H, 4.34; N, 11.93; S, 9.13%. IR (ATR, cm^{-1}): 3032 (νNH), 1562 ($\nu\text{C} = \text{N}$). ^1H NMR (400 MHz, CDCl_3 , δ , ppm): 9.09 (b, 1H, NH), 8.60 (s, 1H, HC = N), 8.31 (s, 1H, Ar-H), 8.10 (d, 2H, Ar-H), 7.98 (d, 2H, 8 Hz, Ar-H), 7.72 (d, 2H, 8 Hz, Ar-H), 7.57–7.55 (m, 5H, Ar-H), 7.43 (d, 1H, 8 Hz, Ar-H), 7.17 (t, 1H, 8 Hz, Ar-H).

2.2.2. 2-(2-(Anthracen-9-ylmethylene)hydrazinyl)quinoline (QHA)

This was prepared from 9-anthracenecarboxaldehyde (0.206 g, 1 mmol) and 2-hydrazinylquinoline (0.159 g, 1 mmol). Yield: 77%. Color: Yellow. M.p.: 195 °C. Anal. Calcd. for $\text{C}_{24}\text{H}_{17}\text{N}_3$: C, 82.97; H, 4.93; N, 12.10. Found: C, 83.02; H, 4.98; N, 12.17%. IR (ATR, cm^{-1}): 3039 (νNH), 1608 ($\nu\text{C} = \text{N}$). ^1H NMR (400 MHz, CDCl_3 , δ , ppm): 9.02 (b, 1H, NH), 8.63 (d, 2H, 8.5 Hz Ar-H), 8.48 (s, 1H, HC = N), 8.02 (d, 3H, Ar-H), 7.67 (d, 2H, Ar-H), 7.56–7.48 (m, 7H), 7.31 (s, 1H, Ar-H).

2.3. General procedure for the synthesis of the ruthenium complexes (1–4)

All the complexes were synthesized by the following general procedure. $[\text{RuHCl}(\text{CO})(\text{E})_3]$ (E = PPh_3 or AsPh_3) or $[\text{RuCl}_2(\text{AsPh}_3)_3]$ (0.1 mmol) was reacted under reflux with 1-(anthracen-10-yl)methylene-2-(benzo[d]thiazol-2-yl)hydrazine (BHA) (0.1 mmol) or 1-((anthracen-10-yl)methylene)-2-(quinolin-2-yl)hydrazine (QHA) (0.1 mmol) in a chloroform-ethanol (20 mL, 1:1 v/v) mixture for 8 h under reflux. Initially an orange color was formed, which gradually changed to red. The completion of the reaction was confirmed by thin layer chromatography (TLC) and the solvent was evaporated in a rotavapor to obtain the crude product. The crude product was then purified by column chromatography using the eluents petroleum ether and ethyl acetate (9:1, v/v).

2.3.1. $[(\text{BHA})\text{RuH}(\text{CO})(\text{PPh}_3)_2]$ (1)

The ligand BHA (0.035 g, 0.1 mmol) was reacted with $[\text{RuHCl}(\text{CO})(\text{PPh}_3)_3]$ (0.095 g, 0.1 mmol) to form complex **1**. Yield: 80%. M.p.: 162 °C. Anal. Calcd for $\text{C}_{59}\text{H}_{45}\text{N}_3\text{OP}_2\text{Ru}$: C, 70.36; H, 4.50; N, 4.17; S, 3.18. Found: C, 70.25; H, 4.46; N, 4.12; S, 3.12%. IR (ATR, cm^{-1}): 1900 (νCO), 1573 ($\nu\text{C} = \text{N}$). ^1H NMR (400 MHz, CDCl_3 , δ , ppm): –13.44 (t, 1H, Ru-H), 8.61 (s, 1H, HC = N), 8.37–6.91 (m, 43H, Ar-H). ^{13}C NMR (100 MHz, CDCl_3 , δ , ppm): 200.89 (CO), 162.11 (C=N), 148.96 (N=C-N), 133.74–124.85 (Ar-C). ^{31}P NMR (162 MHz, CDCl_3 , δ , ppm): 48.52. Calcd ESI-mass (m/z) for $\text{C}_{59}\text{H}_{45}\text{N}_3\text{OP}_2\text{RuS}$: 1007.9. Found: 1008.1 $[\text{M} + \text{H}]^+$. Crystals of complex **1** were grown by the diffusion method with chloroform and ethanol solvents at room temperature.

2.3.2. $[(\text{BHA})\text{RuCl}_2(\text{AsPh}_3)_2]$ (2)

The ligand BHA (0.035 g, 0.1 mmol) was reacted with $[\text{RuCl}_2(\text{AsPh}_3)_3]$ (0.108 g, 0.1 mmol) to form complex **2**. Yield: 75%. M.p.: 192 °C. Anal. Calc for $\text{C}_{59}\text{H}_{45}\text{N}_3\text{SCl}_2\text{As}_2\text{Ru}$: C, 61.22; H, 3.99; N, 3.69; S, 2.82. Found: C, 61.15; H, 3.79; N, 3.62; S, 2.75%. IR (ATR, cm^{-1}): 3305 (νNH), 1577 ($\nu\text{C}=\text{N}$). ^1H NMR (400 MHz, CDCl_3 , δ , ppm): 10.15 (s, 1H, NH), 8.61–6.51 (m, 43H, Ar-H), 8.42 (s, 1H, HC = N). ^{13}C NMR (100 MHz, CDCl_3 , δ , ppm): 162.65 (C=N), 148.03 (N=C-N), 134.84–124.85 (Ar-C). Crystals of complex **2** were grown by the diffusion method with chloroform and ethanol solvents at room temperature.

2.3.3. $[(\text{QHA})\text{RuH}(\text{CO})(\text{PPh}_3)_2]$ (3)

The ligand QHA (0.034 g, 0.1 mmol) was reacted with $[\text{RuHCl}(\text{CO})(\text{PPh}_3)_3]$ (0.095 g, 0.1 mmol) to form complex **3**. Yield: 72%. M.p.: 210 °C. Anal. Calcd for $\text{C}_{61}\text{H}_{47}\text{N}_3\text{OP}_2\text{Ru}$: C, 73.19; H, 4.73; N, 4.20. Found: C, 73.12; H, 4.66; N, 4.13%. IR (ATR, cm^{-1}): 1938 (νCO), 1609 ($\nu\text{C} = \text{N}$). ^1H NMR (400 MHz, CDCl_3 , δ , ppm): –12.41 (t, 1H, Ru-H), 8.33 (s, 1H, HC = N), 8.01–6.59 (m, 45H, Ar-H). ^{13}C NMR (100 MHz, CDCl_3 , δ , ppm): 202.98 (CO), 166.30 (C=N),

144.70 (N=C-N), 134.84–124.65 (Ar-C). ^{31}P NMR (162 MHz, CDCl_3 , δ , ppm): 47.17. Calcd ESI-mass (m/z) for $\text{C}_{61}\text{H}_{47}\text{N}_3\text{OP}_2\text{Ru}$: 1001.3. Found: 1002.1 $[\text{M} + \text{H}]^+$. Crystals of complex **3** were grown by the diffusion method with dichloromethane and petroleum ether solvents at room temperature.

2.3.4. $[(\text{QHA})\text{RuH}(\text{CO})(\text{AsPh}_3)_2]$ (**4**)

The ligand QHA (0.034 g, 0.1 mmol) was reacted with $[\text{RuHCl}(\text{CO})(\text{AsPh}_3)_3]$ (1.085 g, 0.1 mmol) to form complex **4**. Yield: 60%. M.p.: 232 °C. Anal. Calcd for $\text{C}_{61}\text{H}_{47}\text{N}_3\text{OAs}_2\text{Ru}$: C, 67.28; H, 4.35; N, 3.86. Found: C, 67.23; H, 4.30; N, 3.81%. IR (ATR, cm^{-1}): 1908 (νCO), 1615 ($\nu\text{C}=\text{N}$). ^1H NMR (400 MHz, CDCl_3 , δ , ppm): -12.78 (s, 1H, Ru-H), 8.33 (s, 1H, HC = N), 8.09–6.80 (m, 45H, Ar-H). ^{13}C NMR (100 MHz, CDCl_3 , δ , ppm): 203.09 (CO), 166.28 (C=N), 144.15 (N=C-N), 134.84–124.66 (Ar-C). Calcd ESI mass (m/z) for $\text{C}_{61}\text{H}_{47}\text{N}_3\text{OAs}_2\text{Ru}$: 1089.9. Found: 1090.0 $[\text{M} + \text{H}]^+$.

2.4. X-ray crystallography

Crystal data were collected for complexes **1–3** at 296 K using a Gemini A Ultra Oxford diffraction automatic diffractometer. Graphite monochromated Mo-K α radiation ($\lambda = 0.71073 \text{ \AA}$) was used throughout the analysis. Absorption corrections were performed by the multi-scan method. Corrections were made for Lorentz and polarization effects. The structures were solved by the direct method using the program SHELXS 2018 [25]. Refinement and all further calculations were carried out using SHELXL. The H atoms were included in calculated positions and treated as riding atoms using the SHELXL default parameters. Non-hydrogen atoms were refined anisotropically using weighted full-matrix least squares on F 2 . Atomic scattering factors were incorporated in the computer programs.

2.5. Computational studies

2.5.1. Hirshfeld surface analysis

A necessary complete structural description was carried out by Hirshfeld Surface Analysis (HSA), which is used to visualize and quantify the individual types of intermolecular contacts and their impact on crystal packing in the crystal environment. Furthermore, HSA helps to define the occupied space by a molecule and partitions the electron density of the crystal into molecular fragments [26]. The Crystal Explorer 17.5 software was used to calculate the HSA and the respective fingerprint plots at very high resolution for the two coordination complexes with the aid of the Crystallographic Information File (CIF). The d_{norm} plot clearly shows the distances from the outside nuclei surface (d_{e}) and the inside surface (d_{i}); the fixed color scale d_{norm} plot for the three coordination complexes were -0.23 to 0.95; -0.12 to 1.70 and -0.08 to -1.86 Å. The shape index plot was mapped in the color range -1.0 to 1.0 au. In the d_{norm} surface, the sum of the vdw radii was indicated by a white surface, the short contact distances, less than the vdw radii, were displayed by a blue surface and the close-contact interactions (hydrogen bond contacts) were shown by a red surface on the three-dimensional (3D) Hirshfeld surfaces. In the shape index, the blue and red colors reflect the cycle stacking (C-H... π and π ... π interactions). Moreover, the 2D fingerprint plots help to summarize contact distances to the HSA (d_{i} , d_{e}), which shows the range from 0.6 to 2.8 Å, including reciprocal contacts where the different type of intermolecular interactions of the molecule in the crystal can be characterized by the shapes of the fingerprint plots.

2.5.2. Density functional theory

The newly synthesized complexes **1–3** were optimized by B3LYP (DFT) with the 6-311G** basis set [27]. The atomic charges,

HOMO, LUMO and electrostatic potential map have been analyzed from Gaussian03 [28,29], Gauss view [30] and 3D plot software packages [31].

2.6. General procedure for the α -alkylation of ketones

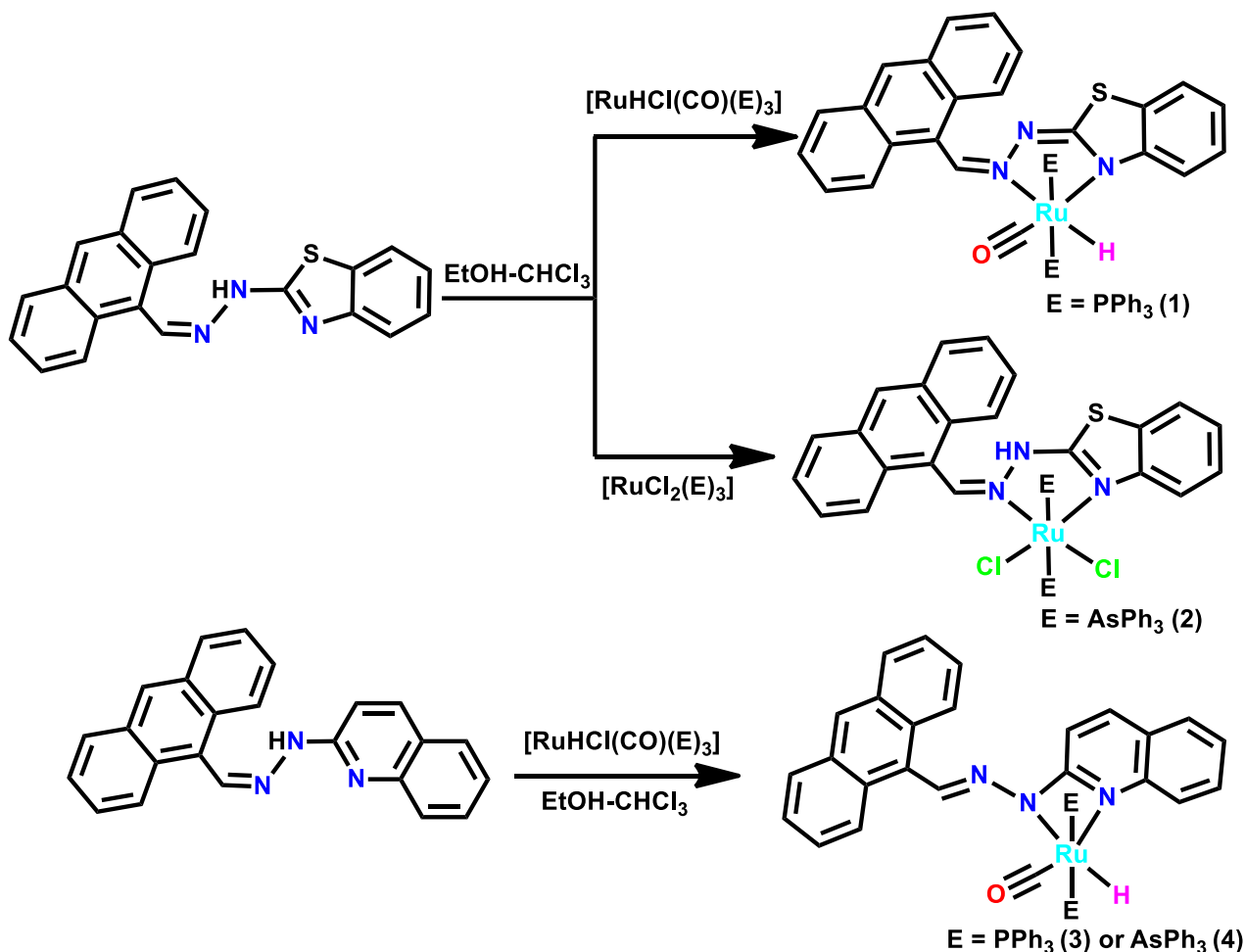
The aromatic ketones (1.5 mmol), aromatic primary alcohols (1.5 mmol), catalyst (1 mol%), KOH (10 mol%) and toluene (5 mL) were charged into a round bottom flask and heated at 110 °C for 12 h. The progress of the reaction was monitored by TLC. Upon completion, the reaction mixture was cooled to room temperature. The catalyst was separated by the addition of a dichloromethane and petroleum ether solvent mixture (1:1 v/v, 20 mL), followed by filtration through celite. The filtrate was concentrated under reduced pressure and the resulting crude product was purified by column chromatography over silica gel (100–200 mesh) with a hexane–ethyl acetate solvent mixture (9.5:0.5, v/v) as the eluent. The resulting products were identified by a comparison with the NMR (^1H and ^{13}C) and mass spectral data from previous reports.

3. Results and discussion

The ruthenium(II) complexes were obtained by the reaction of the ligands with the ruthenium(II) starting material, $[\text{RuHCl}(\text{CO})(\text{E})_3]$ (E = PPh_3 or AsPh_3) or $[\text{RuCl}_2(\text{AsPh}_3)_3]$, in chloroform-ethanol solvent medium under reflux conditions (Scheme 1). The complexes are non-hygroscopic solids for extended periods and are well soluble in organic solvents like methanol, ethanol, dichloromethane, chloroform, 1,4-dioxane, tetrahydrofuran, acetonitrile, dimethylformamide and dimethyl sulfoxide, as well as in non-polar solvents like benzene and toluene. The elemental analyses (C, H, N and S) of the new complexes **1–4** were in good agreement with the expected structures of the ruthenium hydrazone complexes. The ESI mass spectra of the new complexes reveal that the calculated molecular masses are in good accord with the observed molecular masses (Figs. S1–S3 in the supporting information). The results confirm the formation of the desired complexes.

3.1. Spectroscopy studies

The IR spectra furnish preliminary information about the metal ligand bonding. In the spectra of the free ligands, a peak appearing in the region 3307–3305 cm^{-1} was assigned to the hydrazine NH stretching frequency. The NH peak was not present in the spectra of complexes **1**, **3** and **4**, showing that coordination of the ligands to the ruthenium metal takes place by deprotonation either via the hydrazinic nitrogen atom or benzothiazole ring nitrogen atom by amine imine tautomerism. However, in the spectrum of complex **2**, the NH peak did not disappear, revealing the non-participation of the hydrazinic nitrogen atom in coordination. The strong band observed in the spectra of the ligands at 1570–1562 cm^{-1} was assigned to the azomethine group. In the spectra of complexes **1** and **2**, this band shifted to a higher frequency and appeared in the region 1577–1573 cm^{-1} , indicating the participation of the imine nitrogen atom in coordination with the metal. However, the position of the azomethine peak did not change in the spectra of complexes **3** and **4**, depicting the non-participation of the imine nitrogen atom with the metal center. A strong band was observed in the spectra of complexes **1**, **3** and **4** in the region 1938–1900 cm^{-1} which was assigned to a terminally coordinated carbonyl groups, being observed at a slightly higher frequency than in the ruthenium precursor complexes. In addition, the coordinated triphenylphosphine and triphenylarsine ligands showed peaks in the expected regions [32,33].



Scheme 1. Synthesis of the ruthenium(II) complexes 1–4.

The 1H NMR spectra of the ligands and the new complexes confirm the coordination of the ligands with the metal (Figs. S4–S9 in the supporting information). A broad singlet appears at δ 10.70–10.13 ppm in the spectra of the ligands, which was assigned to the hydrazine (NH) proton. This peak was absent in the spectra of metal complexes **1**, **3** and **4**, confirming that coordination of the ligands with the ruthenium metal takes place by deprotonation either via the hydrazinic nitrogen atom or benzothiazole ring nitrogen with the metal. In complex **2**, the NH peak not disappearing reveals the non-participation of the hydrazinic nitrogen atom in coordination. The peak appearing at δ 8.61–8.34 ppm in the spectra of the ligands is due to the imine (HC = N) proton, which shifted downfield and appeared at δ 8.60–8.64 ppm in the spectra of complexes **1** and **2**, showing the participation of the imine nitrogen atom in coordination with the metal. In complexes **3** and **4**, the position of imine proton peak did not change, describing non-participation of the imine nitrogen atom in coordination with the metal. The aromatic protons appeared in the region δ 8.61–6.51 ppm. In addition, for complexes **1**, **3** and **4**, a Ru-H signal appeared in the region δ –13.44 to –12.41 ppm. The ^{13}C NMR spectra show the signals for the coordinated metal complexes in the expected regions (Figs. S10–S13 in the supporting information). The appearance of a peak at δ 202.98–200.89 ppm reveals the presence of a terminal carbonyl group. The peak for the azomethine carbon atom was observed as a singlet at δ 162.65–161.11 ppm. The peak due to the N=C–N carbon atom appeared at δ 145 ppm. Moreover, peaks

for the aromatic carbon atoms were observed in the region δ 133.84–124.65 ppm [34]. The ^{31}P NMR spectra of complexes **1** and **3** were recorded to confirm the presence and configuration of the triphenylphosphine groups (Figs. S14 and S15 in the supporting information). The appearance of sharp singlet at δ 48.52–47.17 ppm suggests the presence of two magnetically equivalent triphenylphosphine groups *trans* to each other [35].

3.2. Molecular structures of complexes 1–3

The solid-state structures of complexes **1–3** have been determined by single crystal X-ray diffraction to confirm the exact coordination modes of the ligands and the geometries around the ruthenium atoms. The crystal data and structure refinement parameters for complexes **1–3** are summarized in Table 1 and selected bond lengths and bond angles are depicted in Table 2. The ORTEP views of complexes **1–3** along with the atomic numbering schemes are given in Figs. 1–3. The single-crystal X-ray studies reveal that complexes **1–3** crystallized in the triclinic system with the space group *Pi*. All the Ru(II) complexes describe a distorted octahedral geometry wherein a bidentate mode is adopted by the ligand, creating five or four membered chelate rings. The remaining apical sites are filled up by carbonyl, chloride or hydride ligands and a pair of PPh_3 or $AsPh_3$ co-ligands, giving CN_2P_2Cl , $N_2As_2Cl_2$ and CN_2P_2H coordination environments. Typically, the PPh_3 or $AsPh_3$ co-ligands prefer to occupy *cis* positions for an enhanced π -interaction, however the presence of a stronger π -acidic CO

Table 1
Crystal data and structural refinement parameters for complexes **1–3**.

	Complex 1	Complex 2	Complex 3
CCDC	1,990,120	1,990,120	1,990,120
Empirical formula	C ₅₉ H ₄₅ ClN ₃ OP ₂ RuS	C ₅₈ H ₄₄ As ₂ Cl ₂ N ₃ RuS	C ₆₁ H ₄₇ N ₃ OP ₂ Ru
Formula weight	1042.50	1136.84	1001.03
Temperature (K)	296(2)	296(2)	296(2)
Wavelength (Å)	0.71073	0.71073	0.71073
Crystal system	Triclinic	Triclinic	Triclinic
Space group	P1	P1	P1
Unit cell dimensions			
a (Å)	13.4920(6)	12.8355(4)	13.0849(3)
b (Å)	14.1831(7)	12.9425(4)	18.0296(5)
c (Å)	15.3520(7)	16.0266(5)	22.0748(6)
α (°)	66.0670(10)	92.345(2)	99.8070(10)
β (°)	81.460(2)	96.154(2)	92.8880(10)
γ (°)	66.4310(10)	106.373(2)	107.6030(10)
Volume (Å ³)	2460.8(2)	2532.63(14)	4862.5(2)
Z	2	2	4
Density (calculated, Mg/m ³)	1.407	1.491	1.367
Absorption coefficient (mm ⁻¹)	0.526	1.794	0.435
F(000)	1070	1146	2064
Crystal size (mm ³)	0.22 × 0.14 × 0.07	0.24 × 0.17 × 0.11	0.240 × 0.170 × 0.070
Theta range for data (°) collection	2.747–28.297	1.281–29.113	2.417–20.808
Index ranges	–17 ≤ h ≤ 17, –18 ≤ k ≤ 18, –20 ≤ l ≤ 20	–17 ≤ h ≤ 17, –17 ≤ k ≤ 17, –21 ≤ l ≤ 21	–13 ≤ h ≤ 13, –18 ≤ k ≤ 18, –22 ≤ l ≤ 22
Reflections collected	11,315	50,726	17,618
Independent reflections	11,315 [R(int) = 0.0104]	13,630 [R(int) = 0.0338]	10,142 [R(int) = 0.0391]
Goodness-of-fit on F ²	0.844	1.033	1.043
Final R indices [I > 2σ(I)]	R1 = 0.0426 wR2 = 0.1270	R1 = 0.0416 wR2 = 0.1185	R1 = 0.0500 wR2 = 0.1233
R indices (all data)	R1 = 0.0499 wR2 = 0.1381	R1 = 0.0703 wR2 = 0.1417	R1 = 0.0650 wR2 = 0.1362
Extinction coefficient	n/a	n/a	n/a
Largest diff. peak and hole (e Å ⁻³)	0.969 and –0.814	1.119 and –1.419	0.597 and –0.330

Table 2
Selected bond lengths and bond angles in complexes **1–3**.

Complex 1	Complex 2	Complex 3
Bond lengths (Å)		
Ru(1)–C(23)	As(2)–Ru(1)	Ru(1)–C(25)
1.842(3)	2.4723(4)	1.834(8)
Ru(1)–N(3)	Ru(1)–N(1)	Ru(1)–N(3)
2.120(2)	2.099(3)	2.163(5)
Ru(1)–N(1)	Ru(1)–N(2)	Ru(1)–N(2)
2.215(2)	2.116(3)	2.180(4)
Ru(1)–P(2)	Ru(1)–Cl(1)	Ru(1)–P(2)
2.3625(7)	2.4176(19)	2.3613(14)
Ru(1)–P(1)	Ru(1)–Cl(2)	Ru(1)–P(1)
2.3617(7)	2.461(2)	2.3669(15)
Ru(1)–H(1A)	Ru(1)–As(1)	Ru(1)–H(1)
1.439(1)	2.4887(4)	1.660
Bond angles [°]		
C(23)–Ru(1)–N(3)	N(1)–Ru(1)–N(2)	C(25)–Ru(1)–N(3)
178.05(12)	77.14(11)	170.2(3)
C(23)–Ru(1)–N(1)	N(1)–Ru(1)–Cl(1)	C(25)–Ru(1)–N(2)
107.21(12)	168.97(8)	110.5(3)
N(3)–Ru(1)–N(1)	N(2)–Ru(1)–Cl(1)	N(3)–Ru(1)–N(2)
74.70(9)	91.96(8)	60.25(17)
C(23)–Ru(1)–P(2)	N(1)–Ru(1)–Cl(2)	C(25)–Ru(1)–P(2)
90.90(9)	96.42(8)	89.7(2)
N(3)–Ru(1)–P(2)	N(2)–Ru(1)–Cl(2)	N(3)–Ru(1)–P(2)
89.48(6)	173.55(8)	87.03(12)
N(1)–Ru(1)–P(2)	Cl(1)–Ru(1)–Cl(2)	N(2)–Ru(1)–P(2)
93.39(6)	94.47(5)	89.46(12)
C(23)–Ru(1)–P(1)	N(1)–Ru(1)–As(2)	C(25)–Ru(1)–P(1)
89.17(9)	89.49(7)	94.2(2)
N(3)–Ru(1)–P(1)	N(2)–Ru(1)–As(2)	N(3)–Ru(1)–P(1)
90.11(6)	91.61(7)	89.64(12)
N(1)–Ru(1)–P(1)	Cl(1)–Ru(1)–As(2)	N(2)–Ru(1)–P(1)
96.19(6)	92.51(4)	92.41(12)
P(2)–Ru(1)–P(1)	Cl(2)–Ru(1)–As(2)	P(2)–Ru(1)–P(1)
169.95(3)	88.60(4)	174.74(6)
H(1)–Ru(1)–C(23)	N(1)–Ru(1)–As(1)	N(3)–Ru(1)–H(1)
90.03	89.40(7)	95.44
N(3)–Ru(1)–H(1A)	N(2)–Ru(1)–As(1)	N(2)–Ru(1)–H(1)
88.11(1)	88.15(7)	155.65(1)
N(1)–Ru(1)–H(1)	Cl(1)–Ru(1)–As(1)	P(1)–Ru(1)–H(1)
162.62(1)	88.58(4)	88.70
P(1)–Ru(1)–H(1)	Cl(2)–Ru(1)–As(1)	P(2)–Ru(1)–H(1)
86.01(1)	91.52(4)	86.45
P(2)–Ru(1)–H(1)	As(2)–Ru(1)–As(1)	H(1)–Ru(1)–C(25)
83.94(1)	178.89(15)	85.46

ligand might have forced the bulky PPh₃/AsPh₃ ligands to take *trans* positions for steric reasons [36,37].

In complex **1**, the ruthenium atom is in a distorted octahedral environment with *trans* angles of [P(1)–Ru(1)–P(2)] 169.96(3)° and [N(1)–Ru(1)–H(1A)] 162.62(1)°. The carbonyl group *trans* to the coordinated N(3) atom [N(3)–Ru(1)–C(23)] gives an angle of 178.05(12). The *trans* angles deviate from linearity and lead to a

small N(1)–Ru(1)–N(3) bite angle of 74.70(9)°. The ruthenium–ligand distances, namely Ru(1)–C(23) 1.842(3) Å, Ru(1)–N(3) 2.120(2) Å, Ru(1)–N(1) 2.215(2) Å, Ru(1)–H(1A) 1.439(1) Å, Ru(1)–P(2) 2.3625(7) Å and Ru(1)–P(1) 2.3617(7) Å, found in the complexes agree well with those reported for similar ruthenium complexes containing triphenylphosphine ligands in *trans* positions [36]. Complex **2** displays a similar type of coordination environment

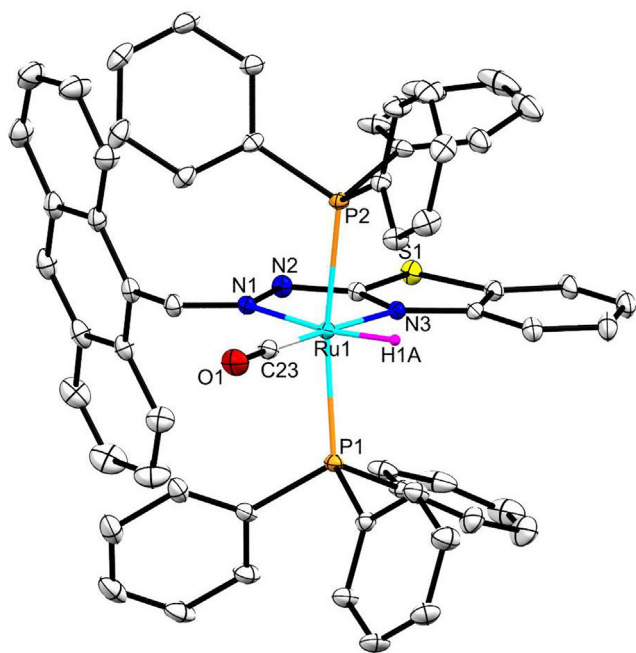


Fig. 1. Perspective view (50% probability ellipsoids) of the complex $[(\text{BHA})\text{RuH}(\text{CO})(\text{PPh}_3)_2]$ (**1**).

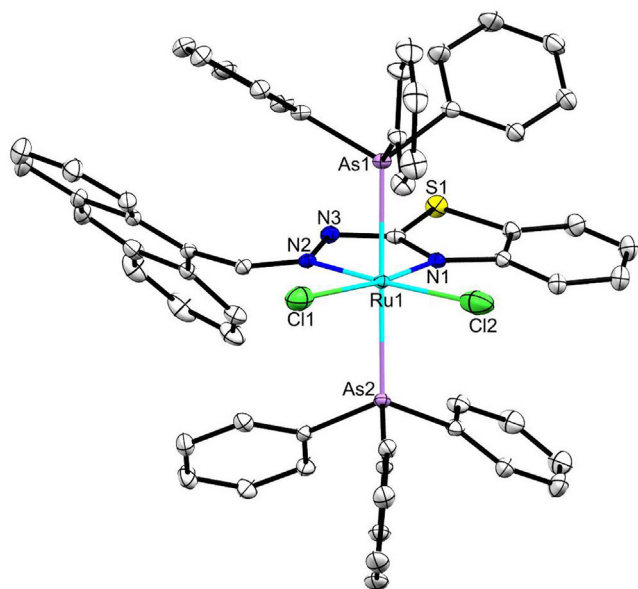


Fig. 2. Perspective view (50% probability ellipsoids) of the complex $[(\text{BHA})\text{RuCl}_2(-\text{AsPh}_3)_2]$ (**2**).

to complex **1**, but with the $[\text{As}(1)-\text{Ru}(1)-\text{As}(2)]$ trans angles of $178.89(15)^\circ$ being higher than the analogous angle in the complex **1**. This is due to presence of steric requirements of the chloride and AsPh_3 ligands. The chloride groups trans to the coordinated N(1) atom, $[\text{N}(1)-\text{Ru}(1)-\text{Cl}(1)]$ and N(2) $[\text{N}(2)-\text{Ru}(1)-\text{Cl}(2)]$, show angles of $168.97(3)$ and $173.55(8)^\circ$. There is no deviation in the trans angles from linearity and this leads to an $\text{N}(2)-\text{Ru}(1)-\text{N}(1)$ bite angle of $77.14(11)^\circ$. The ruthenium–ligand distances, namely, $\text{Ru}(1)-\text{Cl}(1)$ 2.4176(19) Å, $\text{Ru}(1)-\text{Cl}(2)$ 2.461(2) Å, $\text{Ru}(1)-\text{N}(1)$ 2.099(3) Å, $\text{Ru}(1)-\text{N}(2)$ 2.116(3) Å, $\text{Ru}(1)-\text{As}(1)$ 2.4887(4) Å and

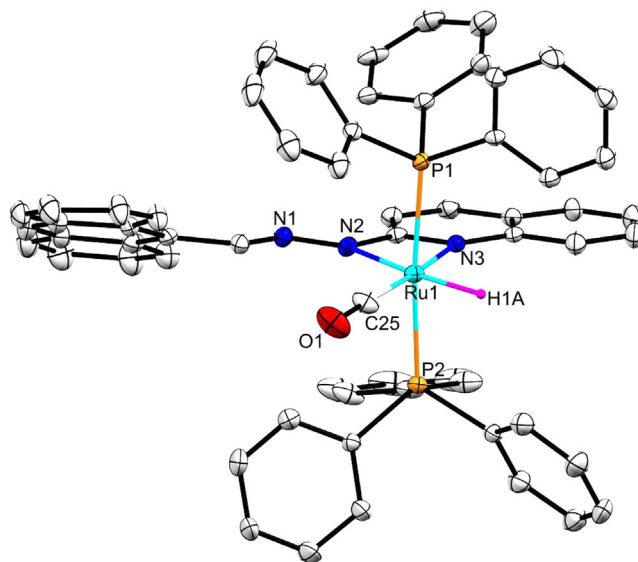


Fig. 3. Perspective view (50% probability ellipsoids) of the complex $[(\text{QHA})\text{RuH}(\text{CO})(\text{PPh}_3)_2]$ (**3**).

$\text{Ru}(1)-\text{As}(2)$ 2.4723(4) Å, found in the complexes agree well with those reported for similar ruthenium complexes containing triphenylarsine ligands in trans positions [38].

In complex **3**, the ligand (QHA) is coordinated to the ruthenium ion as a monoanionic bidentate N,N -donor ligand, forming a more strained four-membered chelate ring with an $\text{N}(2)-\text{Ru}(1)-\text{N}(3)$ bite angle of $60.25(17)^\circ$ (Fig. 3). A number of reasons have been offered as being responsible for the versatility in coordination, such as the bulky quinoline unit restricting rotation about the $\text{N}-\text{N}$ bond. The formation of such a four-membered chelate ring by the QHA ligand and similar ligands is quite normal. The QHA ligand, ruthenium, carbonyl and hydride constitute one equatorial plane of the octahedron, with the metal at the center, and the two triphenylphosphine ligands take up the remaining two axial positions; hence, they are mutually *trans*. The carbonyl ligand is *trans* to the coordinated nitrogen atom of the quinoline moiety and the hydride ion is *trans* to the nitrogen N(2) atom. The $\text{Ru}(1)-\text{H}(1\text{A})$, $\text{Ru}(1)-\text{C}(25)$, $\text{Ru}(1)-\text{P}(1)$ and $\text{Ru}(1)-\text{P}(2)$ distances are 1.660, 1.834(8), 2.3669(15) and 2.3613(14) Å respectively. The observed bond distances are comparable with those found in other reported ruthenium complexes containing PPh_3 ligands [39]. The $\text{Ru}-\text{N}(3)$ length of 2.163 Å is comparable to that found in similar four-membered chelates, whereas the $\text{Ru}-\text{N}(2)$ distance of 2.180 Å is a little longer than usually observed. The elongation of the $\text{Ru}-\text{N}$ bond, which is *trans* to the $\text{Ru}-\text{H}$ bond, may be attributed to the *trans* effect of the hydride ligand.

3.3. Hirshfeld surface analysis

Hirshfeld surface analysis was completed with the purpose of reviewing the nature of the intra and intermolecular interactions, and their contribution to the supramolecular assembly of the complexes. The d_{norm} and shape index of complexes **1–3** are shown in Fig. 4. On comparing the coordination complexes **1–3**, blue and white surfaces are more predominant than red surfaces in all three complexes due to hydrophobic cyclic rings. The dark red and blue surfaces of the shaped index indicate $\text{C}-\text{H} \cdots \pi$ interactions in the crystals. Fingerprint plots are used to quantify the contribution of different types of interactions in the solid state (Fig. 5). The fingerprint plots of all three complexes display interactions that are very

similar. The H···H and C···H types of interactions are highly present in the molecules, which also confirm that vdW and C–H··· π interactions play a major role in the crystal environment. Therefore, this fingerprint plot clearly confirms weak hydrogen bonding that gives stability to all three coordination complexes (**1–3**). The contribution of the H···H and C···H interactions for the molecules are shown in Fig. 5.

3.4. Density functional theory

The Mulliken atomic charges (MPA) of complexes **1–3** were calculated using the Gaussian09 software [29]. Table S1 shows the MPA charges of the atoms of the three complexes. An electrostatic potential map helps to predict the possible reactive sites of the molecule, where nucleophilic (attracted to regions with positive potential) and electrophilic (attracted towards regions with negative potential) regions are present in the molecule. Fig. 6 shows the isosurface representation of the molecular electrostatic potential (MSP) of the metal coordination compounds. Large electronegative regions are found on the surface of the metal coordination region.

Essential quantum chemical descriptors, such as the HOMO and LUMO, were calculated for the three metal coordination complexes (**1–3**) and these are highly related to the chemical and biological activities. The molecular surface of the HOMO and LUMO maps of the three complexes were drawn at 0.2 au and are shown in Fig. 7, in which the HOMO and LUMO energy surfaces of the molecules were found over the metal and functional group regions. The

HOMO is highly localized on the metal centre and its surroundings (Ru, As, P, N and S atoms), and the other regions are very low, whereas in the LUMO, the major contributions are on the phenyl rings and there is minor contribution for the metal centre and its surroundings. The positive and negative regions are shown in green and red colors respectively. In order to understand the charge injection and transporting properties of the metal coordination molecules, the global reactivity descriptors were calculated. The HOMO and LUMO energies rationalise the transfer of charge in a reaction, [35]. The calculated HOMO energies of the complexes vary as **1** (–5.46 eV) > **2** (–5.26 eV) > **3** (–4.47 eV) and those of LUMO exhibit a similar trend: **1** (–1.94 eV) < **2** (–2.29 eV) > **3** (–1.91 eV). The HOMO–LUMO energy gaps in complexes **1** (3.52 eV), **2** (2.96 eV) and **3** (2.57 eV) possess different values, which is consistent with the experimentally observed values. All the calculated global reactivity descriptors are shown in Table 3.

3.5. Catalytic studies

Motivated by their prominent presence in a variety of natural products and pharmaceuticals, as well as in petroleum and biomass feedstocks, considerable research efforts have been focused on the development of catalytic coupling methods with the utilization of ketones and alcohols. Here, the synthesized ruthenium(II) hydrazone complexes have been used as environmentally compassionate catalyst for the formation of C–C coupling products by the α -alkylation of ketones using alcohols. Initially, the α -alkylation reaction was started using the benchmark substrates

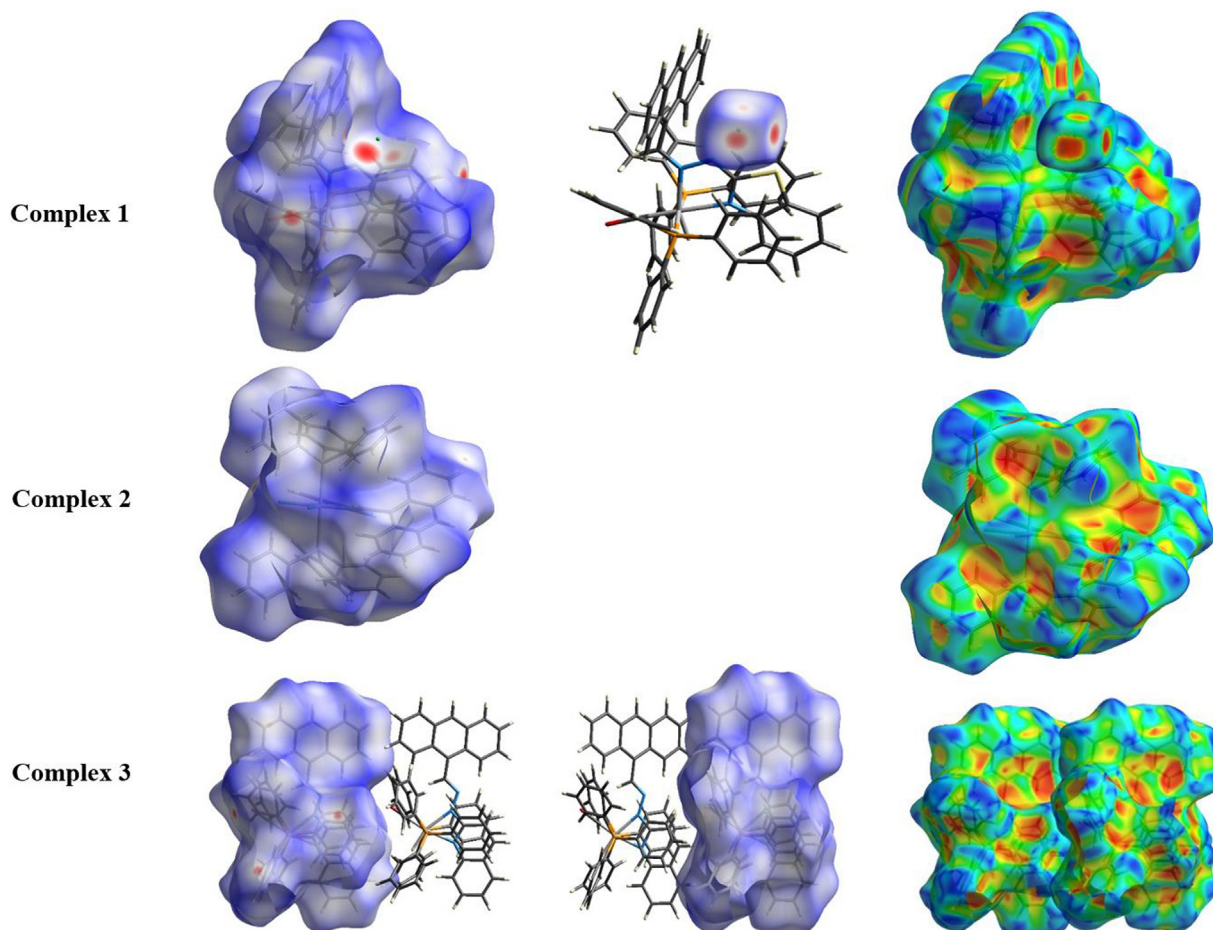


Fig. 4. Hirshfeld surface analysis mapped with d_{norm} and shaped index for complexes **1–3**.

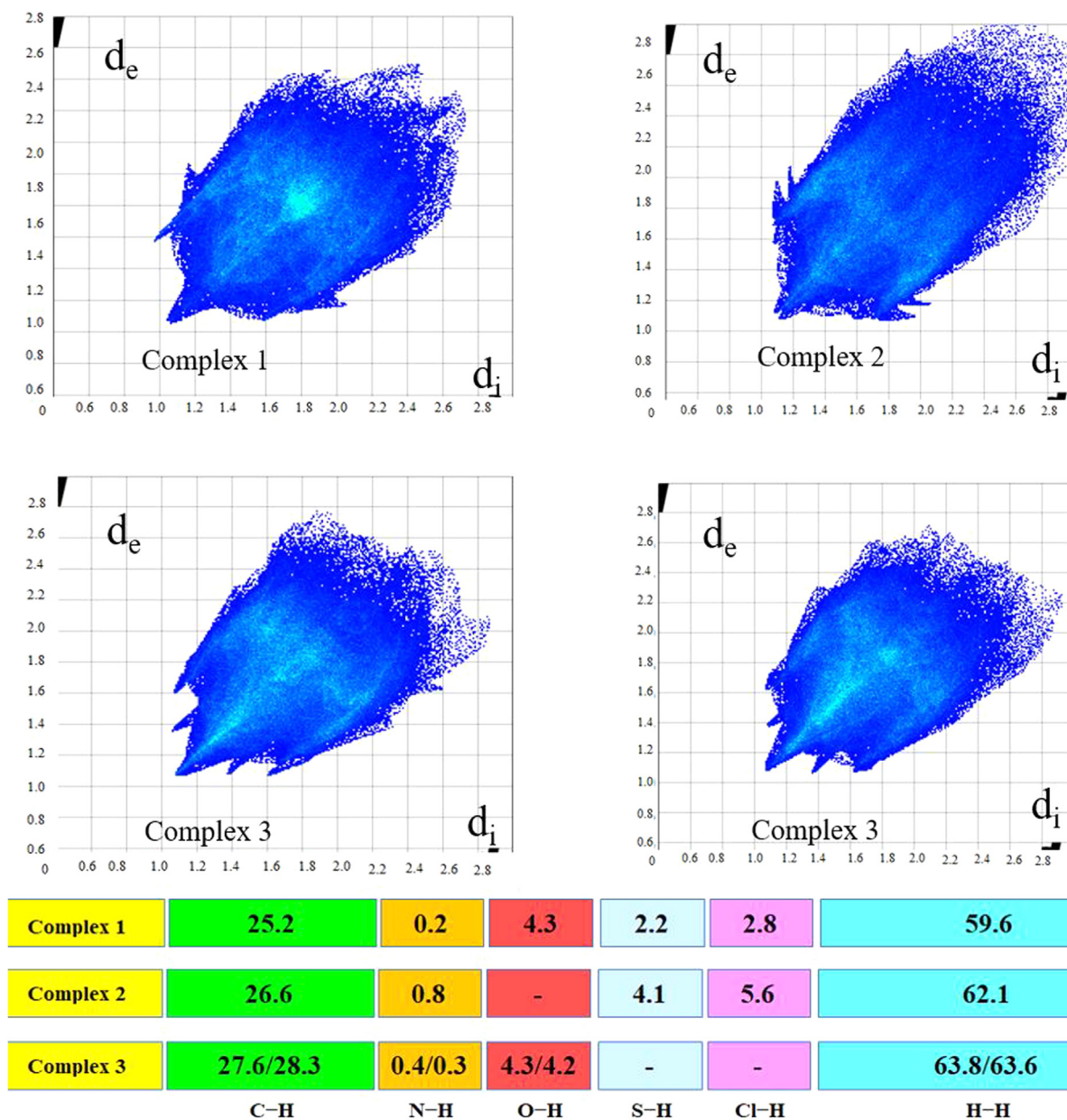


Fig. 5. Fingerprint plot of complexes 1–3, full and resolved into O···H, C···H and H···H contacts, showing the percentages (%) of contacts contributing to the total Hirshfeld surface area of each molecule.

acetophenone and benzyl alcohol, with catalyst **3**. These substrates were selected in order to optimize various conditions, such as the presence of base, solvent, time and catalyst loading for the α -alkylation. The results of the preliminary reactions are shown in Table 4. In order to assess the crucial role of the base in promoting the generation of the metal chalcone intermediate (α , β unsaturated carbonyl) formed in the catalyst cycles, various bases such as Na_2CO_3 , K_2CO_3 , NaHCO_3 , KOH , NaOH and KOTBu were employed to find the best one. Weak bases, such as Na_2CO_3 , K_2CO_3 and NaHCO_3 , were ineffective (Table 4, entries 1–3). The presence of the strong base NaOH led to a higher yield for this reaction (Table 3, entry 5, yield 74%). When the reaction was carried out in the presence of KOH , the α -alkylated product formed in an excellent yield (Table 4, entry 4, yield 94%), hence which we considered this to be the choice for the base. Another strong base, KOTBu , was found to be ineffective (Table 4, entry 6). In the absence of a base, α -alkylation was not observed (Table 4 entry 14). Moreover, the reaction

without the metal catalyst in the presence of a catalytic amount of base showed that the hydrogen borrowing reaction did not occur completely.

In addition to this, we were interested in exploring the solvent dependent activities with the most frequently used solvents, such as toluene, 1,4 dioxane, THF, acetonitrile, benzene, DMF and DMSO (Table 4, entries 1–15). Aromatic hydrocarbon solvents such as toluene and benzene (Table 4, entries 10 and 11) were found to be better reaction media than polar aprotic solvents like DMF and DMSO (Table 4, entries 12 and 13), whereas ether-like solvents, such as THF and dioxane, gave moderate yields (Table 4, entries 7 and 8). The results show that the solvent's polarity and ability to dissolve the reactants and catalyst play a vital role in the efficiency of the catalytic system.

We also explored the significance of catalyst loading and the results are depicted in Table 5. To study the effect of the amount of the catalyst, the reactions were carried out with different

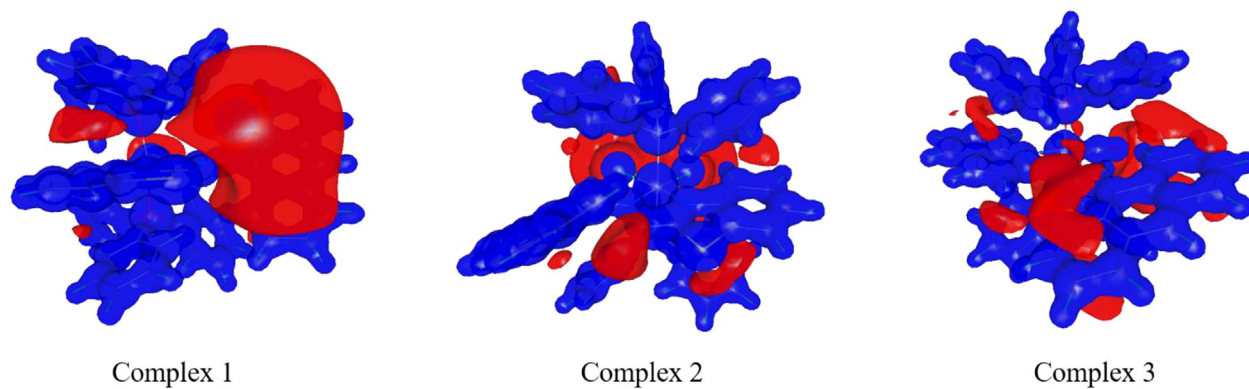


Fig. 6. Isosurface representation of the molecular electrostatic potential of complexes 1–3. Blue: positive potential, Red: negative potential. The surface values are $+0.6$ and -0.06 eÅ⁻¹.

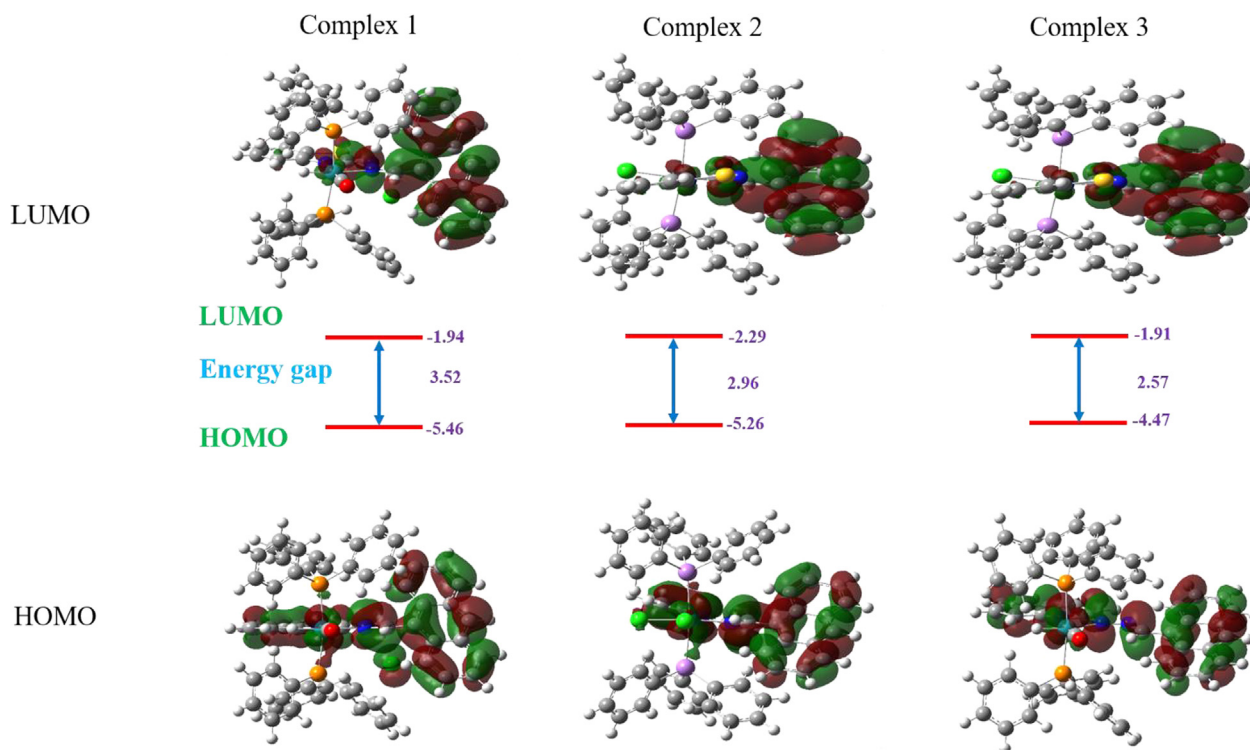


Fig. 7. The highest occupied molecular orbital (HOMO) and the lowest unoccupied molecular orbital (LUMO) of the metal coordination compounds. The HOMOs and LUMOs are drawn at the 0.02 au level.

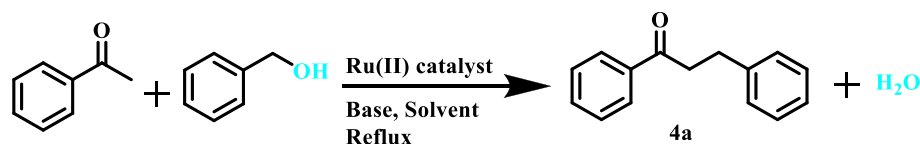
Table 3
Calculated global reactivity properties of the metal complexes 1–3.

Global Reactivity Descriptor	DFT Energy (eV)		
	Complex 1	Complex 2	Complex 3
Band Gap	3.52	2.96	2.57
HOMO Energy	-5.46	-5.26	-4.47
LUMO Energy	-1.94	-2.29	-1.91
Ionization Potential $I = -E_{\text{HOMO}}$	5.46	5.26	4.47
Electron Affinity $A = -E_{\text{LUMO}}$	1.94	2.29	1.90
Global Hardness $\eta = (I - A)/2$	1.76	1.48	1.28
Electronegativity $\chi = (I + A)/2$	3.70	3.78	3.19
Electrophilicity $\omega = \mu^2/2\eta$, $\mu = -\chi$	3.89	4.8	3.96

amounts of catalyst ranging from 0.5 to 1.5 mol %. When the catalyst loading was increased from 0.5 to 1.0 mol % of catalyst **3**, the product yield also increased and reached 94% in 12 h. Increasing of the catalyst load further to 1.5 mol % led to little difference in the yield (Table 5, entry 7). Hence, the optimum catalyst loading was fixed to be 1.0 mol % (Table 5, entry 3). Additionally, catalyst **3** was found to be the best catalyst for the α -alkylation reaction, obtaining an excellent yield (Table 5, entry 3). The other catalysts, **1**, **2** and **4**, showed lower activity than catalyst **3** (Table 4, entries 1, 2 and 4). From the optimization results, it is concluded that 1.0 mol % of catalyst **3** in toluene was sufficient to push this reaction at 110 °C in presence of KOH.

To investigate the substrate scope, we examined the α -alkylation for a variety of aromatic acetophenones with different aromatic

Table 4
Optimization of catalytic conditions for the α -alkylation of acetophenone using benzyl alcohol.^a



Entry	Base	Solvent	T °C	Time (h)	Yield (%) ^b
1	Na ₂ CO ₃	Toluene	110	12	40
2	K ₂ CO ₃	Toluene	110	12	50
3	NaHCO ₃	Toluene	110	12	35
4 ^e	KOH	Toluene	110	12	94
5	NaOH	Toluene	110	12	74
6	KO ^t Bu	Toluene	110	12	67
7	KOH	Dioxane	100	12	75
8	KOH	THF	65	12	72
9	KOH	CH ₃ CN	82	12	45
10	KOH	Toluene	110	14	90
11	KOH	Benzene	80	12	55
12	KOH	DMF	130	12	50
13	KOH	DMSO	140	12	45
14 ^c	–	Toluene	110	24	n.r
15 ^d	KOH	Toluene	110	24	18

^a Acetophenone (1.5 mmol), benzyl alcohol (1.5 mmol), base (10 mol %), catalyst **3** (1 mol%) in solvent (5 mL).

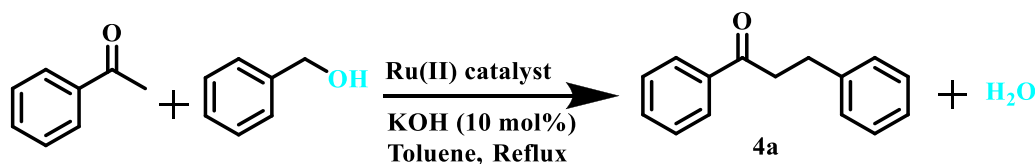
^b Isolated yield after column chromatography.

^c The reaction was carried out without base.

^d The reaction was carried out without catalyst.

^e Better optimization conditions.

Table 5
Influence of substitution and catalyst loading on the α -alkylation of acetophenone with benzyl alcohol.^a



Entry	Catalyst	Amount of catalyst (Mol %)	Yield (%) ^b
1	1	1	85
2	2	1	82
3 ^c	3	1	94
4	4	1	79
5	3	0.5	78
6	3	0.8	87
7	3	1.5	96

^a Acetophenone (1.5 mmol), benzyl alcohol (1.5 mmol), catalyst, KOH (10 mol %) in toluene (5 mL) refluxed at 110 °C for 12 h.

^b Isolated yield after column chromatography.

^c Better optimization conditions.

primary alcohols and the results are shown in Table 6. Our Ru catalytic system was tolerant to various functional groups based on the standard reaction conditions. The reaction of acetophenone with alcohols such as 2-methyl benzyl alcohol, 4-methoxy benzyl alcohol and 2-phenyl ethanol afforded the corresponding products in good yields (Table 6, entries 1–3). Presence of an electron donating group on benzyl alcohol (Table 6, entries 1 and 2) decreased the yield of the product when compared to the unsubstituted alcohol (yield 94%). When *o*-hydroxy acetophenone was reacted with alcohols, the yields of the corresponding products was moderate (Table 6, entries 4–7, yield 76–86%). Steric effects due to the presence of the hydroxy group in the acetophenone plays a role in decreasing the yield of the products. The reaction of 4-methoxy-2-hydroxy acetophenone with alcohols such as benzyl alcohol, 2-methyl benzyl alcohol,

4-methoxy benzyl alcohol and 1-phenyl ethanol afforded the corresponding C–C coupled products in good yields (Table 6, entries 9–11).

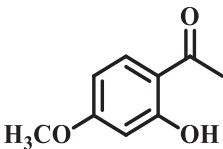
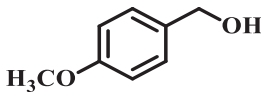
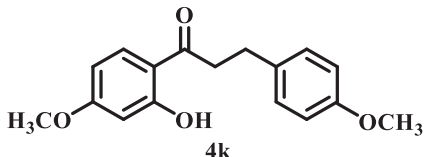
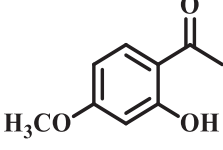
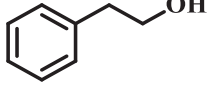
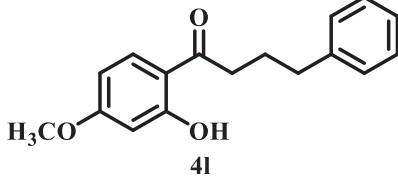
The recyclability of catalyst **3** was studied over 5 runs for the α -alkylation of acetophenone by benzyl alcohol under the optimized conditions. After each run, the catalyst was recovered by the addition of a dichloromethane and hexane mixture. The catalyst was then thoroughly washed with hexane and dried in air before using in the next run. As shown in Fig. 8, the catalyst can be efficiently reused >5 times without any significant loss of catalytic activity or selectivity, but after that the activity slightly decreased. This may be due to incomplete catalyst recovery from the reaction mixture. When compared to previously reported catalysts [40], the present catalyst for the α -alkylation of ketones

Table 6
Evaluations of substrate scope ^a

Entry	Ketone	Alcohol	Product	Yield (%)
1				84
2				91
3				87
4				80
5				76
6				86
7				80
8				85
9				82

(continued on next page)

Table 6 (continued)

Entry	Ketone	Alcohol	Product	Yield (%)
10				93
11				86

^a Ketone (1.5 mmol), alcohol (1.5 mmol), catalyst **3** (1 mol %), KOH (10 mol %) in toluene (5 mL) refluxed at 110 °C for 12 h. ^b Isolated yield after column chromatography.

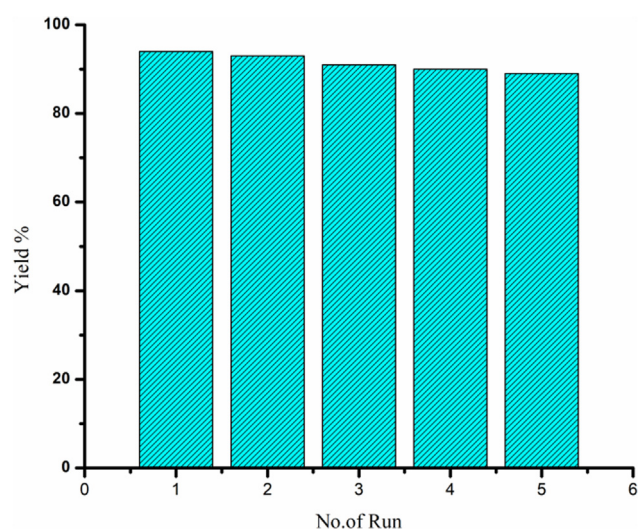


Fig. 8. Recyclability study of catalyst **3** using acetophenone and benzyl alcohol.

with alcohols is more convenient and more efficient since the complex is easier to prepare, cheaper than others and a less amount of catalyst gives a better yield.

4. Conclusions

Novel ruthenium(II) hydrazone complexes were synthesized and characterized by spectroscopic methods. The crystal structures of complexes **1–3** were confirmed by SC-XRD studies, which reveal an octahedral geometry around the Ru metal. The ligands coordinate to Ru(II) ion in a monoanionic bidentate N[−]N fashion in complexes **1**, **3** and **4**, and in a neutral bidentate N[−]N fashion in complex **2**. The crystal lattices of complexes **1–3** were studied using Hirshfeld surface analysis, which shows the presence of several intermolecular interactions, including hydrogen bonds and $\pi \cdots \pi$ stacking interactions. The structural parameters of the complexes obtained by DFT calculations were in good agreement with the X-ray analysis. Complex **3** has the lowest energy gap between the HOMO and LUMO. Moreover, the synthesized complexes were screened as catalysts for the α -alkylation of ketones with alcohols and the results show that complex **3** is an efficient catalyst for the synthesis of the α -alkylation products.

CRediT authorship contribution statement

Kaliyappan Murugan: Conceptualization, Investigation, Writing - original draft. **Subbarayan Vijayapritha:** Validation. **Venkat-achalam Kavitha:** Validation. **Periasamy Viswanathamurthi:** Methodology, Formal analysis, Writing - review & editing, Visualization, Supervision, Project administration.

Declaration of Competing Interest

The authors declare that they have no known competing financial interests or personal relationships that could have appeared to influence the work reported in this paper.

Acknowledgements

We thank the Department of Chemistry, Gandhigram Rural Institute-Deemed University, Gandhigram (NMR spectra), SAIF, Gauhati University, Guwahati (single crystal X-Ray) and CIMF, Periyar University, Salem (single crystal X-Ray) for their help in characterization studies.

Appendix A. Supplementary data

Supplementary data to this article can be found online at <https://doi.org/10.1016/j.poly.2020.114737>.

References

- [1] M.B. Smith, J. March, *March's Advanced Organic Chemistry*, fifth ed., Wiley-Interscience, New York, 2001.
- [2] (a) G. Casiraghi, L. Battistini, C. Curti, G. Rassu, F. Zanardi, *Chem. Rev.* **111** (2011) 3076–3154; (b) C. Palomo, M. Oiarbide, J.M. García, *Chem. Soc. Rev.* **33** (2004) 65–75; (c) P. Arya, H. Qin, *Tetrahedron* **56** (2000) 917–947.
- [3] (a) J. Mlynarski, B. Gut, *Chem. Soc. Rev.* **41** (2012) 587–596; (b) P.H.Y. Cheong, C.Y. Legault, J.M. Um, N. Celebi-Olcum, K.N. Houk, *Chem. Rev.* **111** (2011) 5042–5137.
- [4] (a) F.A. Carey, in: F.A. Carey, R.J. Sundberg (Eds.), *Advanced Organic Chemistry Part B: Reactions and Synthesis*, Springer, New York, 2007, pp. 1–62; (b) J. Otera *Modern Carbonyl Chemistry*, Wiley-VCH, Weinheim, 2000; (c) D. Caine, in: B. M. Trost, I. Fleming (Eds.), *Comprehensive Organic Synthesis*, Vol. 3 Pergamon Press, Oxford, 1991, pp. 1; (d) M. T. Reetz, *Angew. Chem. Int. Ed. Engl.* **21** (1982) 96.
- [5] (a) M.H.G. Prechtel, K. Wobser, N. Theyssen, Y. Ben-David, D. Milstein, W. Leitner, *Catal. Sci. Technol.* **2** (2012) 2039–2042; (b) B. Gnanaprakasam, E. Balaraman, C. Gunanathan, D. Milstein, *J. Polym. Sci. Part A: Polym. Chem.* **50** (2012) 1755–1765; (c) D. Srimani, E. Balaraman, B. Gnanaprakasam, Y. Ben-David, D. Milstein, *Adv. Synth. Catal.* **354** (2012) 2403–2406; (d) A. Tillack, D. Hollmann, D. Michalik, M. Beller, *Tetrahedron Lett.* **47** (2006) 8881–8885; (e) D. Hollmann, A. Tillack, D. Michalik, R. Jackstell, M. Beller, *Chem. Asian J.* **2**

- (2007) 403–410;
- (f) A. Tillack, D. Hollmann, K. Mevius, D. Michalik, S. Bahn, M. Beller, *Eur. J. Org. Chem.* 2008 (2008) 4745–4750;
- (g) M. Zhang, S. Imm, S. Bahn, H. Neumann, M. Beller, *Angew. Chem. Int. Ed.* 50 (2011) 11197–11201;
- (h) M.H.S.A. Hamid, J.M.J. Williams, *Chem. Commun.* 47 (2007) 725–727;
- (i) M.H.S.A. Hamid, J.M.J. Williams, *Tetrahedron Lett.* 48 (2007) 8263–8265;
- (j) M.H.S.A. Hamid, C.L. Allen, G.W. Lamb, A.C. Maxwell, H.C. Maytum, A.J.A. Watson, J.M.J. Williams, *J. Am. Chem. Soc.* 131 (2009) 1766–11744;
- (k) A.J.A. Watson, A.C. Maxwell, J.M.J. Williams, *J. Org. Chem.* 76 (2011) 2328–2331;
- (l) R.N. Monrad, R. Madsen, *Org. Biomol. Chem.* 9 (2011) 610–615;
- (m) K. Yamaguchi, J.L. He, T. Oishi, N. Mizuno, *Chem. Eur. J.* 16 (2010) 7199–7207;
- (n) S. Agrawal, M. Lenormand, B. Martin- Matute, *Org. Lett.* 14 (2012) 1456–1459;
- (o) F.E. Fernández, M.C. Puerta, P. Valerga, *Organometallics* 31 (2012) 6868–6879;
- (p) A.B. Enyong, B. Moasser, *J. Org. Chem.* 79 (2014) 7553–7563;
- (q) E. Balaraman, D. Srimani, Y. Diskin-Posner, D. Milstein, *Catal. Lett.* 145 (2015) 139–144.
- [6] (a) X. Tan, B. Li, S. Xu, H. Song, B. Wang, *Organometallics* 32 (2013) 3253–3261;
- (b) A. Quintard, T. Constantieux, T. Rodriguez, *Angew. Chem. Int. Ed.* 52 (2013) 12883–12887;
- (c) A.M. Zhang, H. Neumann, Beller *Angew. Chem. Int. Ed.* 52 (2013) 597–601;
- (d) M. Zhang, X. Fang, H. Neumann, M. Beller, *J. Am. Chem. Soc.* 135 (2013) 11384–11388;
- (e) J.F. Soule, H. Miyamura, S. Kobayashi, *Chem. Commun.* 49 (2013) 355–357;
- (f) A. Quintard, T. Constantieux, J. Rodriguez, *Chem. Eur. J.* 19 (2013) 14030–14033;
- (g) C. Gunanathan, D. Milstein, *Science* 341 (2013) 249–260;
- (h) M.L. Buil, M.A. Esteruelas, J. Herrero, S. Izquierdo, I.M. Pastor, M. Yus, *ACS Catal.* 3 (2013) 2072–2075;
- (i) L.K. Chan, D.L. Poole, D. Shen, M.P. Healy, *Angew. Chem. Int. Ed.* 53 (2014) 761–765.
- [7] (a) M.S. Kwon, N. Kim, S.H. Seo, I.S. Park, R.K. Cheedra, J. Park, *Angew. Chem. Int. Ed.* 44 (2005) 6913–6915;
- (b) C.S. Cho, B.T. Kim, T.J. Kim, S.C. Shim, *Tetrahedron Lett.* 43 (2002) 7987–7989;
- (c) Y. Iuchi, Y. Obora, Y. Ishii, *J. Am. Chem. Soc.* 132 (2010) 2536–2537;
- (d) T. Kuwahara, T. Fukuyama, I. Ryu, *Org. Lett.* 14 (2012) 4703–4705;
- (e) C. Xu, X. Dong, Z.Q. Wang, X.Q. Hao, Z. Li, L.M. Duan, B.M. Ji, M.P. Song, *J. Organomet. Chem.* 700 (2012) 214–218;
- (f) G. Xu, Q. Li, J. Feng, Q. Liu, Z. Zhang, X. Wang, X.M. Zhang, *Chem. Sus. Chem.* 7 (2014) 105–109;
- (g) F.X. Yan, M. Zhang, X. Wang, F. Xie, M. Chen, H. Jiang, *Tetrahedron* 70 (2014) 1193–1198;
- (h) R. Martínez, G.J. Brand, D.J. Ramón, M. Yus, *Tetrahedron Lett.* 46 (2005) 3683–3686.
- [8] (a) C.S. Cho, B.T. Kim, T. Kim, S.C. Shim, *J. Org. Chem.* 66 (2001) 9020–9022;
- (b) C.S. Cho, B.T. Kim, T. Kim, S.C. Shim, *Tetrahedron Lett.* 43 (2002) 7987–7989;
- (c) C.S. Cho, B.T. Kim, T. Kim, S.C. Shim, *Organometallics* 22 (2003) 3608–3610;
- (d) C.S. Cho, S.C. Shim, *J. Organomet. Chem.* 691 (2006) 4329–4332;
- (e) C.S. Cho, *J. Mol. Catal. A: Chem.* 267 (2007) 49–52;
- (f) C.S. Cho, *J. Mol. Catal. A: Chem.* 240 (2005) 55–60.
- [9] (a) R. Martínez, G.J. Brand, D.J. Ramón, M. Yus, *Tetrahedron Lett.* 46 (2005) 3683–3686;
- (b) R. Martínez, D.J. Ramon, M. Yus, *Tetrahedron* 62 (2006) 8988–9001.
- [10] (a) K. Taguchi, H. Nakagawa, T. Hirabayashi, S. Sakaguchi, Y. Ishii, *J. Am. Chem. Soc.* 126 (2004) 72–73.
- [11] T. Kuwahara, T. Fukuyama, I. Ryu, *Org. Lett.* 14 (2012) 4703–4705.
- [12] S. Liu, L. Xu, C. Liu, Z. Ren, D.J. Young, *J. Lang, Tetrahedron* 73 (2017) 2374–2381.
- [13] F.X. Yan, M. Zhang, X. Wang, F. Xie, M. Chen, H. Jiang, *Tetrahedron* 70 (2014) 1193–1198.
- [14] (a) K. Park, *Angew. Chem. Int. Ed.* 44 (2005) 6913–6915;
- (b) Y.M.A. Yamada, Y. Uozumi, *Org. Lett.* 8 (2006) 1375–1378;
- (c) Y.M.A. Yamada, Y. Uozumi, *Tetrahedron* 63 (2007) 8492–8498;
- (d) X. Cui, Y. Zhang, F. Shi, Y. Deng, *Chem. Eur. J.* 17 (2011) 1021–1028;
- (e) K.I. Shimizu, R. Sato, A. Satsuma, *Angew. Chem., Int. Ed.* 48 (2009) 3982.
- [15] J. Jover, N. Fey, J.N. Harvey, G.C. Lloyd-Jones, A.G. Orpen, G.J.J. Owen-Smith, P. Murray, D.R.J. Hose, R. Osborne, M. Purdie, *Organometallics* 29 (2010) 6245–6258.
- [16] (a) M. Zhang, H. Neumann, M. Beller, *Angew. Chem. Int. Ed.* 52 (2013) 597–601;
- (b) L.M. Geary, J.C. Leung, M.J. Krische, *Chem. Eur. J.* 18 (2012) 16823–16827;
- (c) T.S. Ahmed, R.H. Grubbs, *J. Am. Chem. Soc.* 139 (2017) 1532–1537;
- (d) B.L. Quigley, R.H. Grubbs, *J. Am. Chem. Soc.* 5 (2014) 501–506.
- [17] (a) D.J. Mihalcik, W. Lin, *Angew. Chem. Int. Ed.* 47 (2008) 6229–6232;
- (b) C.S. Gill, K. Venkatasubbaiah, C.W. Jones, *Adv. Synth. Catal.* 351 (2009) 1344–1354.
- [18] S. Syukri, W. Sun, F.E. Kuhn, *Tetrahedron Lett.* 48 (2007) 1613–1617.
- [19] (a) R. Karvembu, R. Prabhakaran, K. Senthilkumar, P. Viswanathamurthi, K. Natarajan, *React. Kinet. Catal. Lett.* 86 (2005) 211–216;
- (b) M. Muthukumar, S. Sivakumar, P. Viswanathamurthi, R. Karvembu, R. Prabhakaran, K. Natarajan, *J. Coord. Chem.* 63 (2010) 296–306.
- [20] (a) R. Ramachandran, G. Prakash, S. Selvamurugan, P. Viswanathamurthi, J.G. Malecki, W. Linert, A. Gusev, *RSC Adv.* 5 (2015) 11405–11422;
- (b) R. Manikandan, P. Anitha, G. Prakash, P. Vijayan, P. Viswanathamurthi, R.J. Butcher, J.G. Malecki, *J. Mol. Catal. A Chem.* 398 (2015) 312–324;
- (c) R. Ramachandran, G. Prakash, S. Selvamurugan, P. Viswanathamurthi, J.G. Malecki, V. Ramkumar, *Dalton Trans.* 43 (2014) 7889–7902;
- (d) G. Prakash, R. Ramachandran, M. Nirmala, P. Viswanathamurthi, W. Linert, *Monatsh Chem.* 145 (2014) 1903–1912.
- [21] A.I. Vogel, *Text Book of Practical Organic Chemistry*, fifth ed., Longman, London, 1989.
- [22] N. Ahmed, J.J. Levison, S.D. Robinson, M.F. Uttley, *Inorg. Synth.* 15 (1974) 45–64.
- [23] A. Sanchez-Delgado, W.Y. Lee, S.R. Choi, Y. Cho, M.J. Jun, *Trans. Met. Chem.* 16 (1991) 241–244.
- [24] T.A. Stephenson, G. Wilkinson, *J. Inorg. Nucl. Chem.* 28 (1996) 945–956.
- [25] G.M. Sheldrick, *Acta Crystallogr. A.* 64 (2008) 112–122.
- [26] (a) M.A. Spackman, D. Jayatilaka, *Cryst EngComm.* 11 (2009) 19–32;
- (b) M.A. Spackman, J.J. McKinnon, *Cryst. Eng. Comm.* 4 (2002) 378–392;
- (c) M.A. Spackman, J.J. McKinnon, D. Jayatilaka, *Cryst. Eng. Comm.* 10 (2008) 377–388;
- (d) M.A. Spackman, J.J. McKinnon, D. Jayatilaka, *Chem. Comm.* 37 (2007) 3814–3816;
- (e) J.J. McKinnon, M.A. Spackman, A.S. Mitchell, *Acta Crystallogr. B* 60 (2004) 627–668.
- [27] (a) E. Wimmer, in: *Density Functional Methods in Chemistry*, Springer, New York, 1991, pp. 7–31;
- (b) R.G. Parr, R.G. Pearson, *J. Am. Chem. Soc.* 105 (1983) 7512–7516;
- (c) R.G. Parr, L.V. Szentpaly, S. Liu, *J. Am. Chem. Soc.* 121 (1999) 1922–1924;
- (d) R.G. Parr, W. Yang, *Density-Functional Theory of Atoms and Molecules*, Oxford Univ. Press, New York, 1989.
- [28] R.E. Davidson, D. Feller, *Chem. Rev.* 86 (1988) 661–696.
- [29] M. J. Frisch, G. W. Trucks, H. B. Schlegel, G. E. Scuseria, M. A. Robb, J. R. Cheeseman, J. A. Montgomery, J. Vreven, K. N. Kudin, J. C. Burant, J. M. Millam, S. S. Iyengar, J. Tomasi, V. Barone, B. Mennucci, M. Cossi, G. Scalmani, N. Rega, G. A. Petersson, H. akatsuji, M. Hada, M. P. Ehara, K. Toyota, R. Fukuda, J. Hasegawa, M. Ishida, T. Nakajima, Y. Honda, O. Kitao, H. Nakai, M. Klene, X. Li, J. E. Knox, H. P. Hratchian, J. B. Cross, J. B. Adamo, J. Jaramillo, R. Gomperts, R. E. Stratmann, O. Yazyev, A. J. Austin, R. Cammi, C. Pomelli, J. W. Ochterski, P. Y. Ayala, Morokuma, G. A. Voth, P. Salvador, J. J. Dannenberg, V. G. Zakrzewski, S. Dapprich, A. D. Daniels, M. C. Strain, O. Farkas, D. K. Malick, A. D. Rabuck, K. Raghavachari, J. B. Foresman, J. V. Ortiz, Q. Cui, A. G. Baboul, S. Clifford, J. Cioslowski, B. B. Stefanov, G. Liu, A. Liashenko, P. Piskorz, I. Komaromi, R. L. Martin, D. J. Fox, T. Keith, M. A. Al-Laham, C. Y. Peng, A. Nanayakkara, M. Challacombe, P. M. W. Gill, B. Johnson, W. Chen, M. W. Wong, C. Gonzalez, J. A. Pople, Gaussian, Inc., Wallingford CT, 2005..
- [30] R. Dennington, T. Keith, J. Millam, GaussView, Version 5, Semichem Inc. 2009..
- [31] A.I. Stash, V.G. Tsirelson, *J. Appl. Cryst.* 47 (2014) 2086–2089.
- [32] (a) D. Bansal, R. Gupta, *Dalton Trans.* 45 (2016) 502–507;
- (b) D. Bansal, G. Kumar, G. Hundal, R. Gupta, *Dalton Trans.* 43 (2014) 14865–14875.
- [33] R. Prabhakaran, P. Kalaivani, R. Huang, M. Sieger, W. Kaim, P. Viswanathamurthi, F. Dallemer, K. Natarajan, *Inorg. Chim. Acta.* 376 (2011) 317–324.
- [34] S. Selvamurugan, R. Ramachandran, G. Prakash, P. Viswanathamurthi, J.G. Malecki, A. Endo, *J. Organomet. Chem.* 803 (2016) 119–127.
- [35] P. Vijayan, P. Viswanathamurthi, P. Sugumar, M.N. Ponnuswamy, M.D. Balakumaran, P.T. Kalaichelvan, K. Velmurugan, R. Nandhakumar, R.J. Butcher, *Inorg. Chem. Front.* 2 (2015) 620–639.
- [36] (a) L.T. Ghoochany, S. Farsadpour, Y. Sun, W.R. Thiel, *Eur. J. Inorg. Chem.* (2011) 3431–3437;
- (b) P. Vijayan, P. Viswanathamurthi, P. Sugumar, M.N. Ponnuswamy, J.G. Malecki, K. Velmurugan, R. Nandhakumar, M.D. Balakumaran, P.T. Kalaichelvan, *Appl. Organomet. Chem.* 31 (2017) 1–23.
- [37] M. Ganeshpandian, R. Loganathan, E. Suresh, A. Riyasdeen, M.A. Akbarsha, M. Palaniandavar, *Dalton Trans.* 43 (2014) 1203–1219.
- [38] P. Kalaivani, R. Prabhakaran, P. Poornima, F. Dallemer, K. Vijayalakshmi, V. Vijayapadma, K. Natarajan, *Organometallics* 31 (2012) 8323–8332.
- [39] R. Ramachandran, G. Prakash, M. Nirmala, P. Viswanathamurthi, J.G. Malecki, *J. Organomet. Chem.* 791 (2015) 130–140.
- [40] R. Wang, L. Huang, Z. Du, H. Feng, *J. Organomet. Chem.* 846 (2017) 40–43.